PNAS RESEARCH ARTICLE | ENGINEERING
BIOPHYSICS AND COMPUTATIONAL BIOLOGY

Robust acoustic trapping and perturbation of single-cell microswimmers illuminate three-dimensional swimming and ciliary coordination

Mingyang Cui[a,b], Susan K. Dutcher[c], Philip V. Bayly[a], and J. Mark Meacham[a,1]

Edited by Howard Stone, Princeton University, Princeton, NJ; received November 5, 2022; accepted April 18, 2023

We report a label-free acoustic microfluidic method to confine single, cilia-driven swimming cells in space without limiting their rotational degrees of freedom. Our platform integrates a surface acoustic wave (SAW) actuator and bulk acoustic wave (BAW) trapping array to enable multiplexed analysis with high spatial resolution and trapping forces that are strong enough to hold individual microswimmers. The hybrid BAW/SAW acoustic tweezers employ high-efficiency mode conversion to achieve submicron image resolution while compensating for parasitic system losses to immersion oil in contact with the microfluidic chip. We use the platform to quantify cilia and cell body motion for wildtype biciliate cells, investigating effects of environmental variables like temperature and viscosity on ciliary beating, synchronization, and three-dimensional helical swimming. We confirm and expand upon the existing understanding of these phenomena, for example determining that increasing viscosity promotes asynchronous beating. Motile cilia are subcellular organelles that propel microorganisms or direct fluid and particulate flow. Thus, cilia are critical to cell survival and human health. The unicellular alga *Chlamydomonas reinhardtii* is widely used to investigate the mechanisms underlying ciliary beating and coordination. However, freely swimming cells are difficult to image with sufficient resolution to capture cilia motion, necessitating that the cell body be held during experiments. Acoustic confinement is a compelling alternative to use of a micropipette, or to magnetic, electrical, and optical trapping that may modify the cells and affect their behavior. Beyond establishing our approach to studying microswimmers, we demonstrate a unique ability to mechanically perturb cells via rapid acoustic positioning.

microswimmers | cilia and flagella | acoustofluidics | acoustic tweezers

The motion of cilia and flagella is critical to the propulsion of microswimmers and the directed movement of physiological fluids, but the mechanisms responsible for this motion remain a mystery. In humans, coordinated beating of motile cilia drives fluid flow in airways, cerebral ventricles, and the oviduct. Ciliary dysfunction is implicated in a range of ciliopathies that include primary ciliary dyskinesia, chronic otitis media, chronic obstructive pulmonary disease, and infertility (1–6). The cytoskeletal structure of cilia (i.e., the 9+2 axoneme comprising nine outer microtubule doublets and two central singlets) is now known in exquisite detail, but the relationship between its form and function is not fully understood (7, 8).

The unicellular alga *Chlamydomonas reinhardtii*, which shares the highly conserved 9+2 axonemal structure with human cilia, is widely used to study ciliary dynamics (9, 10). Biciliate wildtype *C. reinhardtii* cells swim with a characteristic "breaststroke" cilia motion, achieving forward movement via synchronized power and recovery strokes at beat frequencies of 50 to 80 Hz (11, 12). In addition, a slight nonplanarity of the asymmetric beat pattern yields a slow rotation of the cell (at ~2 Hz) about the major body axis (12–14). The resultant motion is complicated, and its full description requires imaging the rhythmically beating cilia with high temporal and spatial resolution. For prolonged observation of ciliary beating in *C. reinhardtii*, a micropipette is commonly used to hold the cell body; however, physical contact constraints rotational degrees of freedom, precluding characterization of the helical navigation that is critical to cell sensing of environmental gradients (15, 16). Micropipette-based capture is difficult and tedious as *C. reinhardtii* cells swim approximately ten body lengths per second (~100 μm/s), and the inability to simultaneously trap multiple cells makes high-throughput studies impractical.

We developed and applied "acoustic tweezers" incorporating ultrasonic surface acoustic waves (SAW) with bulk acoustic waves (BAW) to gain new insight into ciliary motion and coordination. Noncontact trapping enables three-dimensional (3D), torque-free manipulation of a swimming cell. Optical tweezers are commonly used to manipulate

Significance

Acoustic trapping and manipulation of single-cell microswimmers was achieved using ultrasonic standing waves in microfluidic chambers. Bulk acoustic waves produced high trapping forces at low input power, while high-frequency, short-wavelength surface acoustic wave actuation provided the high temporal (milliseconds) and spatial (submicron) resolution needed to characterize three-dimensional body motion and cilia waveform of swimming *Chlamydomonas reinhardtii* cells. Critically, noncontact acoustic trapping did not constrain body rotation or cilia motion. Studies using our hybrid acoustic tweezers revealed effects of temperature and viscosity on swimming characteristics and cilia beating, as well as remarkable robustness of beating to mechanical perturbation. The ability to acoustically trap and perturb strongly swimming microorganisms can be transformative in numerous applications in biology, biomedicine, and biophysics.

Author contributions: M.C., S.K.D., P.V.B., and J.M.M. designed research; M.C. performed research; M.C. and J.M.M. analyzed data; and M.C., S.K.D., P.V.B., and J.M.M. wrote the paper.

The authors declare no competing interest.

This article is a PNAS Direct Submission.

[1]To whom correspondence may be addressed. Email: meachamjm@wustl.edu.

This article contains supporting information online at https://www.pnas.org/lookup/suppl/doi:10.1073/pnas.2218951120/-/DCSupplemental.

Published June 12, 2023.

passive nano-/microparticles (17), but application to active matter, and particularly living cells, is less routine. Long-term optical trapping and analysis of single motile *Escherichia coli* bacteria cells have been reported (18, 19). Optical trapping has also been used to characterize *C. reinhardtii* force dynamics (20); however, measurements of swimming parameters deviated from previously reported ranges. This suggests that optical trapping may affect swimming behavior, for example by perturbing the cilia motion and/or *via* localized heating (21). Like micropipette trapping, optical traps are difficult to multiplex, so analysis of multiple trapped cells is time-consuming. Other noncontact approaches are used to trap and manipulate passive bioparticles, but most have proven ineffective for applications involving microswimmers due to insufficient trapping forces, thermal effects, or other practical limitations (21–23). Active methods may exploit electrical charge or polarizability (electrophoretic and dielectrophoretic trapping) (24, 25) or magnetic susceptibility (magnetic tweezers) (26–28) to distinguish and hold target particles. If particles do not respond directly to the externally applied field, field-sensitive labels (e.g., immunospecific magnetic particles) are needed (29, 30), which could affect biological function or viability (31, 32). In this context, acoustic tweezers have emerged as a compelling alternative that offers noncontact, label-free trapping with high biocompatibility (33–36).

Acoustic tweezers are "gentle", as ultrasound has a negligible impact on cell viability and phenotype (33, 37). Acoustic trapping performance depends on the intrinsic acoustophysical properties of the cells (size, density, and compressibility) through the acoustic contrast factor relative to the suspension medium. No labeling or modification of the cells or medium is needed. Acoustic tweezers employ either BAW or SAW depending on application-specific requirements for spatial resolution and efficiency, as well as fabrication complexity, cost, and size. Applications of acoustofluidic manipulation in biology and biomedicine have grown exponentially (38, 39), but there are few reports on trapping of motile microorganisms (40–44). A larger acoustic radiation force is needed to overcome the propulsive force of the microswimmers; without careful control, the corresponding increase in input power could lead to heating that might damage cells or affect behavior.

In the reported work, high trapping force at low input power was achieved with hybrid acoustic tweezers that use standing surface acoustic waves (SSAW) to drive a standing bulk acoustic wave (SBAW) field for multiplexed trapping and analysis of swimming *C. reinhardtii* cells. The approach breaks the frequency limitation of traditional BAW (< ~10 MHz) to provide the higher efficiency of BAW with the higher resolution of SAW. This hybrid BAW/SAW approach provides an array of trapping sites using a single SAW actuator. Thus, single *C. reinhardtii* cells are rapidly trapped at high throughput, with sufficient temporal and spatial resolution to study ciliary dynamics without altering the function of the cells or cilia. Cilia motion is quantified using an approach previously applied to uniciliated mutants that rotate in place without confinement (45). Here, acoustic trapping enables experiments with wildtype biciliates, allowing us to study coordination of the two cilia and differences between them. First, we describe acoustic field–microswimmer interactions in our devices, using populations of *C. reinhardtii* cells to map the BAW field for various microfluidic chamber geometries and operating conditions. We confirm that temperature-controlled ultrasound exposure does not affect ciliary beat patterns. Noncontact trapping is then applied to assess 3D helical swimming of wildtype *C. reinhardtii*, and to investigate synchronization of the two cilia known as *cis* and *trans* in media with varying viscosity. We find that the body rotation rate is proportional to ciliary beat frequency, which increases linearly with temperature. Increasing viscosity favors asynchronous beating to support in-plane body rotation that would otherwise be suppressed by viscosity. Finally, we demonstrate acoustic positioning (e.g., shifting the nodal location *via* frequency switching) of uniciliate *uni1* mutant cells to study how the cilium responds to mechanical perturbation during swimming.

Results

Hybrid BAW/SAW Acoustofluidic Devices Can Confine Individual Swimming *C. reinhardtii* Cells. We showed previously that traditional PDMS channel-based SAW devices are unable to trap swimming *C. reinhardtii* cells due to a too weak acoustic radiation force acting on the cells (44). Conversely, a one-dimensional (1D) standing BAW driven by SAW in a glass channel-based device achieved a force sufficient to sort *C. reinhardtii* cells without thermal damage. In such devices, BAW develop as SAW leak into the microfluidic channel and reflect off the high acoustic impedance sidewalls of the glass superstrate to form a BAW field. SAW actuation is matched to a BAW channel resonance for efficient operation. In the present work, a single pair of interdigitated transducers (IDTs) generated SSAW in one coordinate direction; however, a square glass microchamber oriented at 45° to the SAW propagation direction supported two overlapping orthogonal SBAW to yield a two-dimensional (2D) array of pressure nodal trapping sites (Fig. 1 *A*–*C*). Particles with positive acoustic contrast factor, such as *C. reinhardtii* cells, polystyrene beads, and SW620 tumor cells, were pushed to these pressure nodes where they became confined (see grids of nodes formed at a drive frequency f_{ac} = ~6.6 MHz for an ~545 μm square chamber, Fig. 1*C*).

Active *C. reinhardtii* cells swim within an ultrasonic standing wave field with the local field either assisting or impeding the motion of a cell depending on the orientation of the acoustic radiation force $\boldsymbol{F}^{rad}$ to the direction of the swim force $\boldsymbol{F}^{swim}$ (Fig. 1*D* and *SI Appendix*). In regions where the field strength exceeds the propulsive capability of the cells, cells will amass at the acoustic pressure nodes (43, 46). If the mode exhibits one or more isolated nodes, single cells can be confined to these locations. We fabricated IDTs that target operating frequencies of ~6.6 MHz, ~8.1 MHz, ~9.6 MHz, and ~19.4 MHz. SSAW formed SBAW fields in chamber shapes that supported resonances at these frequencies. For example, the side lengths of square glass chambers were chosen as ~545 μm for operating frequencies under 10 MHz, and ~275 μm for an operating frequency of ~19.4 MHz.

Microswimmer Distribution Reflects the Strength and Shape of the Acoustic Field. Because the patterns of swimming cells are dictated by the changing acoustic field, *C. reinhardtii* cells can be used as real-time probes of acoustofluidic device performance (43, 46). Populations of these microswimmers were used to visualize and identify resonances for single-cell trapping in various chamber shapes. Devices with square chambers exhibited stable grid patterns with 5 × 5 (f_{ac} = 6.7 MHz, power P_{ac} = 160 mW), 6 × 6 (8.1 MHz, 143 mW), or 7 × 7 (9.6 MHz, 64 mW) pressure nodes (Fig. 1*E* and Movie S1). The smaller chamber of the 19.4 MHz device was also designed to form a 7 × 7 array; however, some expected nodes were absent from the observed pattern, and others appeared to be merged (Fig. 1*F*). The internodal distance can be reduced by using devices that operate at higher frequencies, but the influence of rounded corners becomes more pronounced for square chambers isotropically etched in glass. The power needed to tightly pattern the *C. reinhardtii* cells was

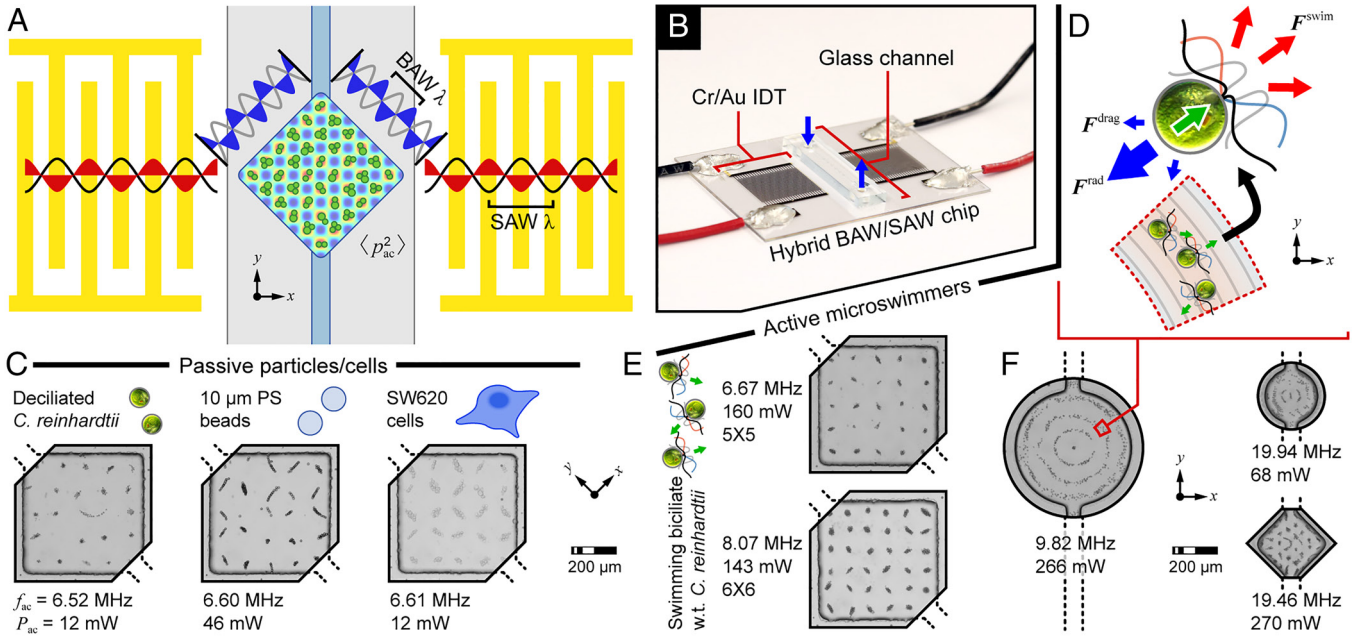

Fig. 1. Acoustic tweezers incorporating two-dimensional (2D) bulk acoustic waves (BAW) driven by one-dimensional (1D) surface acoustic wave (SAW) actuation. (*A*) Illustration of hybrid BAW/SAW device for patterning cell populations and trapping single-cell microswimmers, and (*B*) assembled device. (*C*) Patterning of various passive particles/cells. (*D–F*) Microswimmer confinement to acoustic potential minima of BAW fields driven by SAW actuators. Note that the internodal spacing of the 2D patterns reflects the wavelength of BAW at the reported actuation frequencies.

approximately 5 to 10× that used to pattern the passive particles, ranging from 40 to 300 mW (drive voltage 4 to 15 V_{pp}). This is still considered low for a SAW-driven device, evidencing the efficiency of the hybrid BAW/SAW approach (40, 44). 1D IDTs could also form more complicated 2D pressure fields, creating a pattern with three concentric rings around a central point for both ~9.6 MHz and ~19.4 MHz devices with circular chambers (Fig. 1*F* and Movie S2). As expected, cells near the center of the chamber were more tightly confined than those near the periphery due to the *r*-axial component of the mode shape (46, 47). The capability to drive complex 2D BAW fields using a single 1D SAW actuator offers the higher precision of SAW acoustofluidic devices, without sacrificing the efficiency of BAW devices, in which the field is shaped by the chamber. Cilia dynamics were stable during 60-s actuation periods at multiple cooling stage set point temperatures (*SI Appendix*, Fig. S3, and below). Thus, this noncontact method provides a long observation window relative to the timescale for swimming (milliseconds to seconds). Based on population dynamics, acoustically trapped cells exhibited no damage after release from 10 min confinement, even without use of a cooling stage. This is consistent with earlier studies using acoustic tweezers in various biomaterial trapping applications (40), suggesting that the acoustic tweezers provide long-duration, effective trapping of microswimmers without exceeding their thermotolerance threshold of 37 to 40 °C (48). These results validate the use of living probes to determine optimal operating conditions for hybrid BAW/SAW devices; they also confirm the versatility and biocompatibility of this acoustofluidic approach.

Single-Cell Per Well Acoustic Tweezers Enable Waveform Analysis in Locally Free Swimming Biciliate *C. reinhardtii* Cells. The ~9.6 MHz square chamber device was used for single-cell trapping and cilia waveform analysis. The acoustic trap enabled long-term monitoring of individual *locally free swimming* biciliate cells, which is not possible using earlier methods. Here, "locally-free swimming" is used to describe a condition where the mechanics of swimming via propulsive cilia are unaltered while cells are trapped. The cells can (locally) move with six degrees of freedom, including rotation about three axes and translation, albeit limited by the trap, in three directions. High-resolution microscopy necessitated the use of an oil immersion objective, which increased system losses and thus the power needed to tightly confine a swimming cell (256 mW vs. 64 mW for the air objective). In addition, a coverslip thickness thin glass superstrate was used in place of the thick glass mask blank shown in Fig. 1*B* (*SI Appendix*, Fig. S1). Cilium angle θ_c (sub-c denotes a cilium parameter), beating amplitude $\theta_c^{SD} = \mathrm{std}(\theta_c)$, and curvature κ_c were used to characterize cilia waveform for the *cis* (proximal to the eye spot) and *trans* cilia of biciliate *C. reinhardtii* and the single cilium of *uni1* mutant cells (see definitions in Fig. 2 and *SI Appendix*, Table S1 and *SI Appendix* for a description of analytical methods).

Beat frequency f_c was calculated as the inverse of time lag corresponding to the peak autocovariance in θ_c; the height of the peak covariance was a measure of periodicity. For synchronously beating biciliate wildtype cells, f_c of both cilia was approximately 60 Hz (n = 30; see Table 1 for comparison of parameters for all cilia), whereas uniciliated cells beat at a slightly higher frequency ($f_{c,uni}$ = 67 Hz; n = 30). Note that for cells exhibiting purely synchronous beating, it was not possible to differentiate between the *cis* and *trans* cilia so results for 15 cells with 30 cilia are grouped, i.e., the measured beat frequency is assigned to both cilia. The bend amplitude of $\theta_{c,wt}^{SD} = 0.90$ rad for wildtype cells was slightly higher than for *uni1* where $\theta_{c,uni}^{SD} = 0.81$ rad. The average curvature (averaged over the length of the cilium and a full cycle of beating) $\overline{\kappa}_{c,wt} = -0.18$ rad/μm for wildtype cells, and for *uni1*, $\overline{\kappa}_{c,uni} = -0.20$ rad/μm. These waveform parameters are consistent with previously reported values (45).

During the observation period, synchronous beating of many cells was interrupted by an asynchronous beating period termed a "slip" motion (49, 50) that also distinguished the *trans* cilium

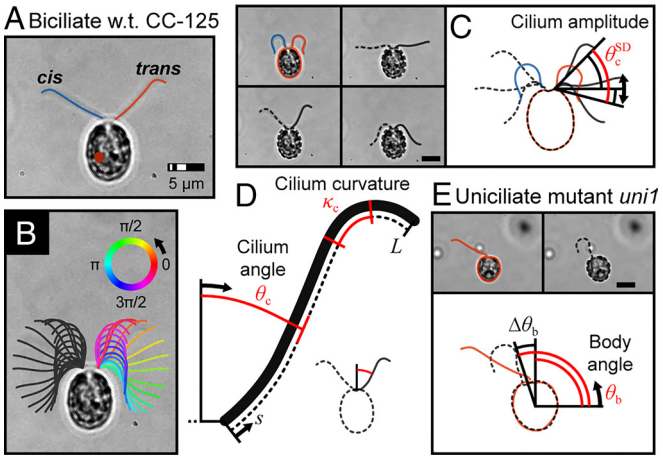

Fig. 2. Schematics of biciliate wildtype (strain CC-125) and uniciliate mutant (strain *uni1*) *C. reinhardtii* cells held in the acoustic tweezers. (*A*) Identification of *cis* and *trans* cilia for biciliate cells. (*B*) Ciliary shapes at equidistant times representing a complete beat cycle ($t \approx 17$ ms). (*C* and *D*) Definitions of cilium amplitude, angle, and curvature. (*E*) Definition of body angle for *uni1* cells.

(Movies S3 and S4 illustrate synchronous vs. asynchronous beating for acoustically confined biciliate cells). Here, the *trans* cilium had a 30% faster average beat frequency than the unchanging *cis* cilium ($f_{c,trans\text{-}async} = 77$ Hz vs. $f_{c,trans\text{-}sync} = 64$ Hz and $f_{c,cis} = 59$ Hz; $n = 12$; Table 1 and Fig. 3*C*), reaching a maximum of ~89 Hz (inverse of shortest beat period) for the transient slip process. Average bend amplitude decreased by ~10% ($\theta^{SD}_{c,trans-async} = 0.80$ rad vs. $\theta^{SD}_{c,trans-sync} = 0.87$ rad and $\theta^{SD}_{c,cis} = 0.90$ rad; Table 1 and Fig. 3*D*), and the mean curvature increased by a slightly smaller amount ($\overline{\kappa}_{c,trans-async} = -0.20$ rad/μm vs. $\overline{\kappa}_{c,trans-sync} = -0.19$ rad/μm and $\overline{\kappa}_{c,cis} = -0.18$ rad/μm ; Table 1 and Fig. 3*E*). The lower amplitude and higher curvature indicate a compressed *trans*-cilium waveform during the asynchrony, which agrees with previous observations of slip motion (Fig. 3 *A* and *B*) (49).

In general, the cilia of biciliates and uniciliates have different beat frequencies and waveforms. However, during asynchronous beating, the *trans* cilium of the wildtype cells more closely resembles the single cilium of the uniciliated *uni1* mutant strain. These observations are also consistent with the understanding of the *uni1* mutation, which preferentially affects assembly of the cilium found in the *cis* position meaning that the *uni1* cilium is usually in the *trans* position (51). Studies with *uni1* cells test the influence of acoustic trapping on cilia beating dynamics. While trapped in an acoustic field, all cells showed a slight elevation in ciliary beat frequency with no detectable change in waveform (*SI Appendix*, Fig. S2); the change in frequency can be attributed entirely to a slight increase in temperature (~1 °C) and not to any change in mechanical loading of the cilia, an effect that is quantified in the *SI Appendix*, Fig. S3 and supported by the helical motion analysis below. Thus, these example studies demonstrate the applicability of our hybrid acoustic tweezers for various investigations of ciliary motion that require high-resolution (< 500 nm) image capture.

Table 1. Summary of waveform parameters for cilia of biciliate wildtype (strain CC-125) and uniciliate mutant (strain *uni1*) *C. reinhardtii* cells

Cilium		f_c (Hz)	θ_c^{SD}(rad)	$\overline{\kappa}_c$(rad/μm)
uni1		67.2 ± 10.6	0.81 ± 0.07	−0.20 ± 0.03
CC-125 sync		60.8 ± 8.7	0.90 ± 0.04	−0.18 ± 0.04
CC-125 async	*cis*	59.0 ± 5.4	0.90 ± 0.04	−0.18 ± 0.03
	trans-sync	63.8 ± 5.7	0.87 ± 0.04	−0.19 ± 0.04
	trans-async	76.8 ± 5.8	0.80 ± 0.03	−0.20 ± 0.03

*Note: all values given as mean ± SD.

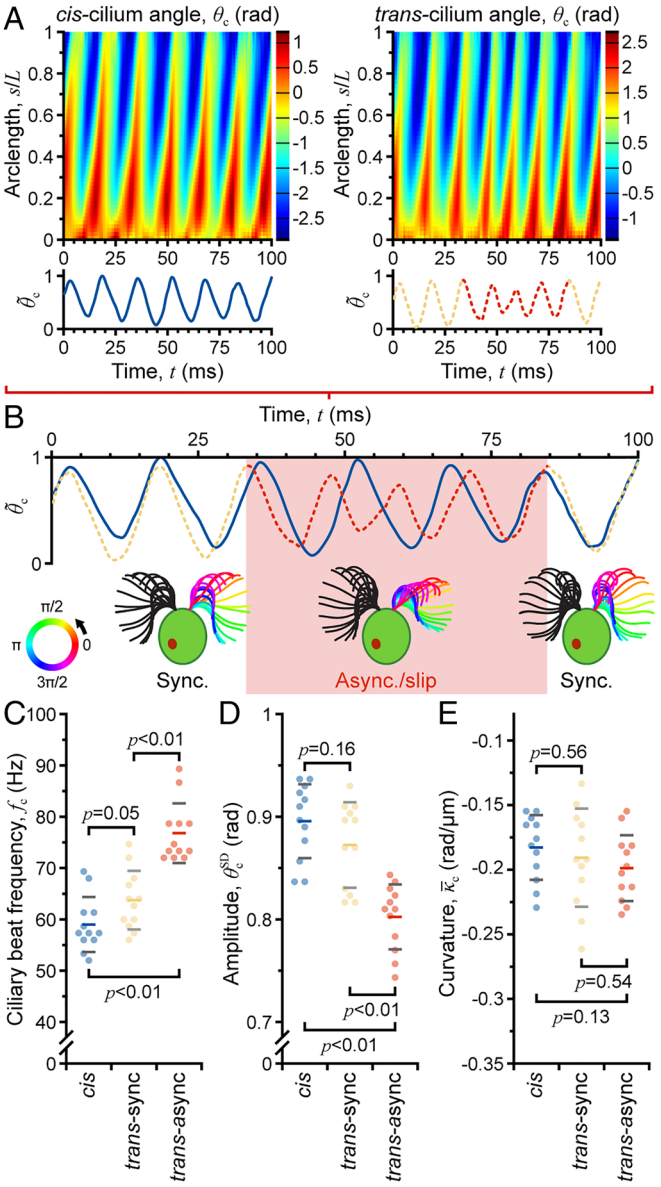

Fig. 3. Characterization of ciliary beat asynchrony during long-term acoustic trapping. (*A*) Beat periodicity using normalized average cilium angle $\tilde{\theta}_c$ vs. time [average determined from map of θ_c vs. nondimensional space (arclength *s*/*L*; *y* axis) and time (*x* axis)]. (*B*) Identification of *cis-trans* beat asynchrony. (*C–E*) Comparison of ciliary waveform parameters beat frequency f_c, amplitude θ_c^{SD}, and mean curvature $\overline{\kappa}_c$ for synchronous and asynchronous beating.

Helical Body Rotation and Cilia Beat Frequency Increase with Temperature at the Same Rate. Microorganisms swim to explore their fluidic world, often following 3D helical trajectories around their primary body axis. The corkscrewing motion is a ubiquitous strategy for eukaryote cells to interrogate gradients in external stimuli (e.g., light, gravity, and chemicals), as this motion lends a periodicity to signals detected by subcellular sensors (eyespots, biological gyroscopes, and surface receptors) (14). For *C. reinhardtii* cells, ciliary beating is essential to control cell reorientation and navigation relative to photostimuli. Wildtype biciliated *C. reinhardtii* cells swim along left-handed helices in a

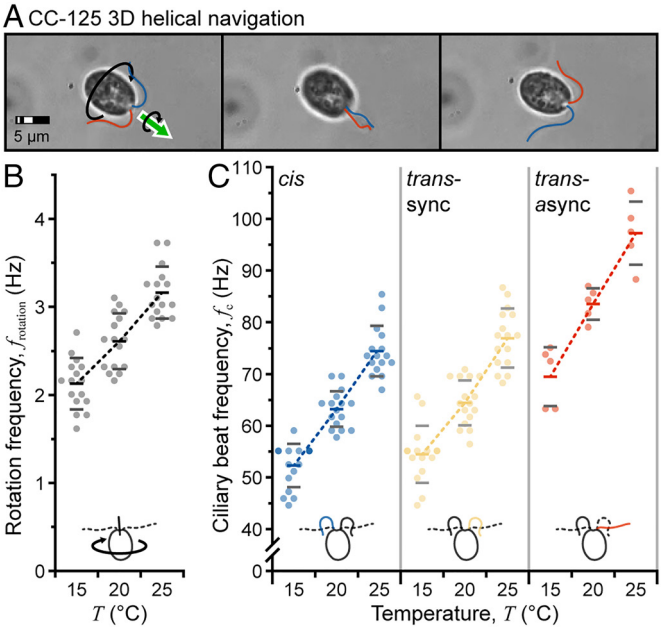

Fig. 4. Measurement of 3D body rotation. (*A*) Sequence of images following one-body inversion (half of a complete rotation). (*B* and *C*) Comparison of *C. reinhardtii* body rotation rate $f_{rotation}$ and ciliary beat frequency f_c with increasing temperature *T*.

breaststroke mode, rotating the body at 2 to 3 Hz (13, 14). The eyespot scans the environment, and cell motion is adjusted based on periodic shading (52); however, the mechanism underlying the helical motion is not fully understood. A recent study and model suggested that the helical motion is caused by an asymmetry in biciliate driving forces, but measurements required that cells be physically constrained using a micropipette (14). Because they impart negligible torque, our acoustic tweezers are uniquely suited to investigate such phenomena. The *uni1* mutant cells were used to confirm that acoustic manipulation was virtually torque-free. For these cells, in-plane rotation rate was unchanged (acoustics on, 2.99 ± 0.74 Hz; acoustics off, 3.09 ± 0.73 Hz; $p = 0.23$), and no out-of-plane rotation was observed. Acoustically confined wildtype *C. reinhardtii* cells were imaged to quantify and compare variations in helical rotation and beat frequency with increasing temperature.

Rotation frequency was first determined manually using the inverse of the time required for twelve body inversions (six complete rotations; one inversion is shown in Fig. 4*A*). At 20 °C, the rotation frequency $f_{rotation}$ was ~2.6 Hz (mean ± SD: 2.61 ± 0.32 Hz; $n = 16$) as shown in Fig. 4*B*, within the accepted range reported by other groups (note that the ideal temperature range for *C. reinhardtii* cells is 20 °C to 32 °C) (12, 13). At 15 °C, $f_{rotation}$ = 2.12 ± 0.29 Hz ($n = 16$; Movie S5), and at 25 °C, $f_{rotation}$ = 3.16 ± 0.30 Hz ($n = 16$; Movie S6), indicating an ~0.5 Hz (~20%) increase with every 5 °C increase in temperature. Repeating the analysis on the *cis* and *trans* cilia (during synchronous and asynchronous beating) showed similar increases in beat frequency with increasing temperature of ~18%, ~17%, and ~17% for these cases, respectively (Fig. 4*C*). These results are comparable and suggest that the increase in beat frequency is almost entirely responsible for the observed increase in body rotation frequency. Because bend amplitude and curvature were relatively unaffected by the increase in temperature (*SI Appendix*, Fig. S4), this confirms that the offset between cilia forces is also not affected by temperature. Thus, our results support the conclusion that asymmetry in biciliate driving forces underlies helical motion while adding new details to the understanding of 3D swimming by *C. reinhardtii* cells.

Increasing Viscosity Decreases Synchronization of *C. reinhardtii* Cilia. Mechanical loading on cilia can be adjusted by increasing the viscosity of the cell medium. This experimental perturbation has been shown to dramatically alter cilia dynamics (53–56). The hybrid BAW/SAW acoustic tweezers enable investigation of swimming behavior under changing environmental conditions (e.g., physical and chemical medium composition, or other external stimuli). Here, we investigate the effect of viscosity on swimming behavior.

Ten cells exhibiting synchronous and asynchronous beating were analyzed for each of four medium viscosities, η = 1 cP, 3 cP, 5 cP, and 8 cP. Because the ciliary beat frequency drops significantly with viscosity, swimming was recorded for different time periods: 200 frames (0.1 s) for 1 cP and 3 cP, 400 frames (0.2 s) for 5 cP, and 800 frames (0.4 s) for 8 cP. For each viscosity, analyses were performed separately for *cis*, *trans*-sync (*trans* cilium synchronously beating with the *cis* cilium), and *trans*-async cilia. In all cases, the beat frequency decreased with increasing viscosity (Fig. 5). Even during synchronous beating, the measured *trans* cilium beat frequency was slightly higher than that of the *cis* cilium due to the effect of sync/async transitions within the observation window. As viscosity was further increased beyond 3 cP, synchronous beating was no longer observed, and "slips" between *trans* and *cis* cilia became more pronounced, i.e., there was ~1 slip per *cis*-cilium beat for $\eta \leq 3$ cP but ~4 slips per *cis*-cilium beat for $\eta = 8$ cP (Movies S7 and S8 compare beating under low and high viscosity conditions). Further, beating became less periodic, and the waveform was less planar based on differences in focal depth along the cilia. Waveform analysis of *cis* and *trans* cilia showed that amplitude first decreased with increasing viscosity from 1 cP to 5 cP, followed by a slight increase at 8 cP (Fig. 5, see *Insets* for representative waveforms). The curvature response was less clear, gradually decreasing for the *cis* cilium and remaining relatively steady for the *trans* cilium. This differs from findings previously reported for uniciliate mutant cells (55), possibly because viscous loading is different for spinning *uni1* cells than for forward-swimming biciliate cells. Although *cis* and *trans* cilia exhibited similar trends in beat frequency (decreasing) and cilium amplitude (decreasing), the two cilia behaved quite differently as viscosity exceeded ~3 cP with both coordination and slip motion being affected. Thus, this study complements prior investigation of the effects of viscosity on the ciliary waveform with *uni1* (55) and newly demonstrates that viscous resistance promotes asynchronous beating in biciliate cells. The increase in asynchrony with viscosity encourages (or maintains) in-plane body rotation that would otherwise be inhibited by viscosity.

Cilia Dynamics Are Insensitive to Rapid Acoustic Translation of the Cell Body. The cilia response to a transient mechanical stimulus was investigated using uniciliate *uni1* mutant cells. Dilute cell suspensions were loaded into the fluidic chamber, and the device was actuated for 0.1 s causing a rapid translation of cells toward the closest acoustic pressure node. The six cells having the highest velocity (275.8 ± 41.6 μm/s, ~3× normal swimming) were selected for analysis.

The rotation speed of three cells increased during the translational movement (a representative case is shown in Fig. 6*A*), while that of the other three decreased (Fig. 6*B*). The direction of change depended on the orientation of the cell body (defined by its major axis, positive toward the end nearest the cilium) relative to the direction of motion. If the cell axis was aligned with the acoustic radiation force, the translation reinforced the power stroke, increasing the rotation rate (Fig. 6*A* and Movie S9). If the cell axis pointed in a direction opposite to the acoustic radiation force, the rotation rate was depressed

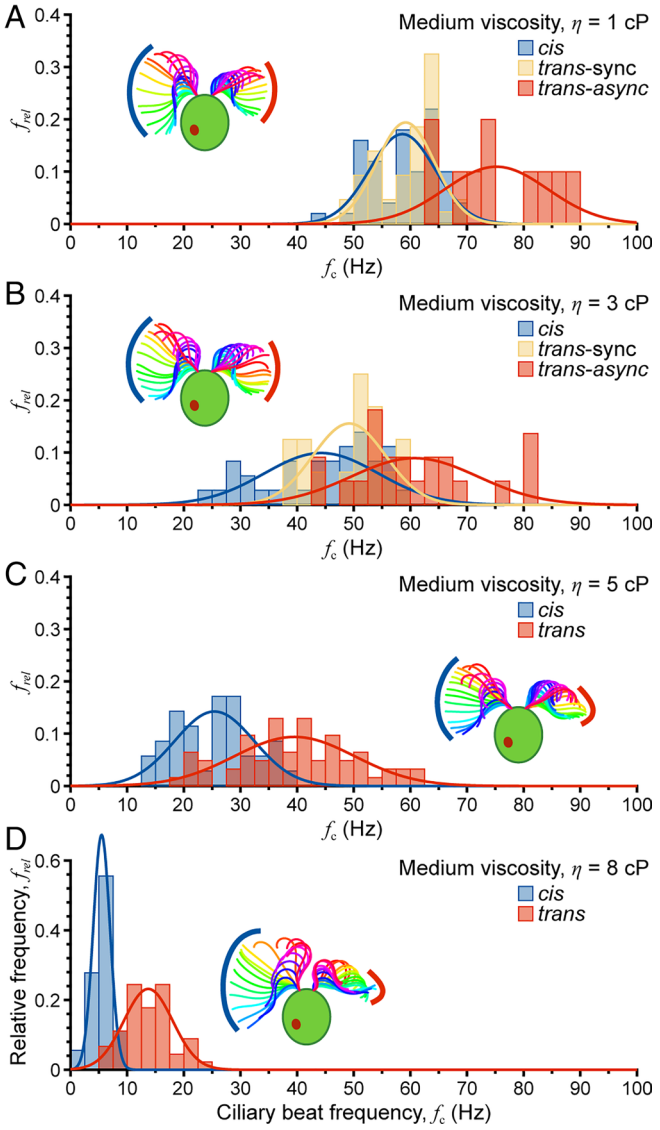

Fig. 5. Effect of viscosity on ciliary beat synchrony. (*A–D*) As medium viscosity is increased from η = 1 cP to η = 8 cP, synchronization decreases until only asynchronous beating is observed for $\eta \geq 5$ cP. Note f_{rel} is the relative frequency of occurrence of cells with a particular beat frequency.

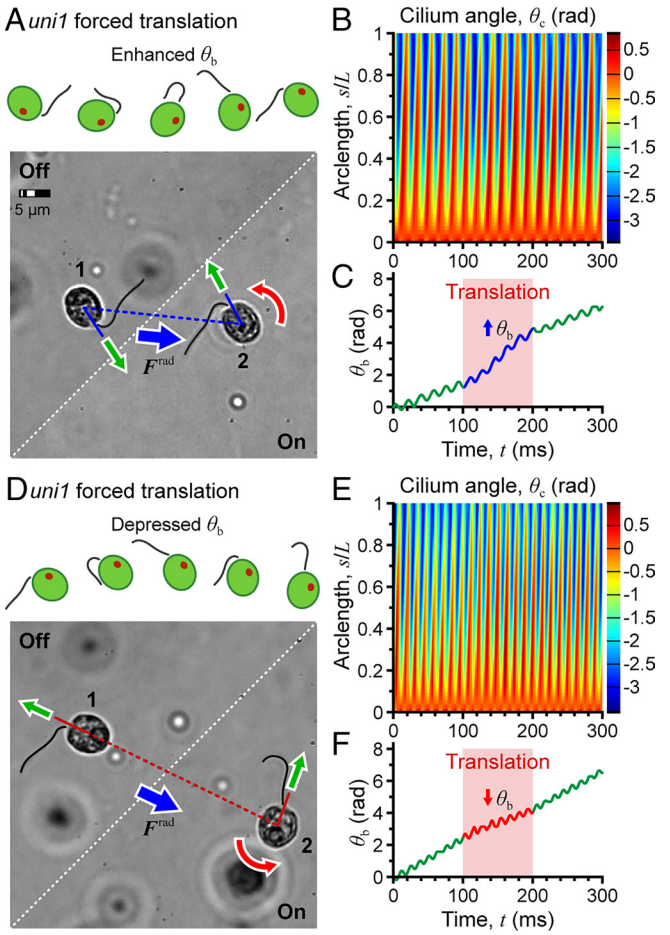

Fig. 6. Acoustic perturbation for rapid translation of the cell body. (*A–C*) Cell axis aligned with the acoustic radiation force, enhancing the rotation rate of the cell body. (*D–F*) Cell axis oriented opposite the acoustic radiation force, depressing the rotation rate.

(Fig. 6*B*). Thus, cell body rotation was either assisted or inhibited by the forced translation of the cell, providing a means to assess the response of the cell swimming and cilium dynamics to mechanical perturbation. In all cases, normal beating of the cilium recovered immediately after removal of the drive signal with no discernible transient, suggesting that cilia dynamics are extremely stable.

Discussion

Hybrid BAW/SAW acoustic tweezers enable the study of single-cell microswimmers with high temporal and spatial resolution. SAW actuation provides *high spatial resolution*, overcoming the low frequency (long wavelength) limitation of traditional BAW systems. Complementing this high resolution, the BAW field supported by the glass superstrate provides *larger acoustic radiation forces* than typical SAW-based devices. Such high efficiency energy transfer is critical to trapping vigorous microswimmers like *C. reinhardtii* without excessive heating (44). Noncontact acoustic confinement can thus fix the cell body in space without affecting the waveform of propulsive cilia. Because the standing acoustic wave applies minimal torque on the body, these acoustic tweezers enable characterization of complex 3D swimming behavior, such as the effect of temperature on beat frequency and helical body rotation. Our device is also compatible with oil immersion microscopy, enabling observation of the dynamics of cilia during what is effectively free swimming, which revealed changes in cilia waveform in response to perturbation of the mechanical environment of the cells (viscosity). The ability to monitor ciliary motion while continuously varying the chemical, mechanical, or optical environment of a cell could open new avenues of cilia research, allowing direct observation of changes in 3D waveform and swimming in response to various stimuli. These acoustic tweezers can also controllably perturb a swimming cell, offering additional possibilities for characterization of cell and cilia dynamics. Finally, these devices are not limited to applications involving *C. reinhardtii*. The BAW/SAW acoustic tweezers can readily be adapted to investigate other microswimmers for a wide range of applications in biology, biomedical engineering, and biophysics. Our approach should be generally applicable when high-spatial resolution focusing and/or trapping are desired, including organoid assembly, investigating cell-to-cell interactions, isolating bacteria and other water contaminants, and trapping active and passive engineered particles.

Materials and Methods

Device Design, Fabrication, and Testing. The glass microfluidic channel dimensions are designed to match BAW resonances with the SAW device resonance. The hybrid BAW/SAW systems are fabricated through standard photolithography for IDT and glass channel patterning, metal lift-off for IDT formation, wet etching for channel creation, and adhesive bonding. *C. reinhardtii* cells were used to characterize the resonance of each device as described previously (43, 46). Briefly, chambers were loaded with wildtype *C. reinhardtii* cells (strain CC-125), and IDTs were actuated over a narrow frequency band around the design frequency while monitoring the evolving cell distribution density. Details of device fabrication and the experimental setup can be found in the *SI Appendix*, Fig. S1.

Cell Culture and Sample Preparation. *C. reinhardtii* cells were obtained from the Dutcher Lab at Washington University in St. Louis. The colorectal cancer line SW620 was obtained from the Fields Lab at Washington University in St. Louis. Details of cell culture and cell preparation can be found in the *SI Appendix*.

Experimental Setup and Microscopy. A function generator (33522A, Agilent) and amplifier (125A250, Amplifier Research) were used to drive the SAW devices. Distributions of cell populations under actuation were imaged using 10× and 20× air objectives. Single-cell trapping was imaged using phase-contrast microscopy with an oil immersion objective lens (100×) to achieve the highest optical resolution for imaging ciliary waveform. Details of the imaging methodology can be found in the *SI Appendix*.

Cilia Dynamics Characterization. Cilia dynamics were analyzed in multiple steps using custom MATLAB scripts. Details of the analysis can be found in the *SI Appendix*.

Data, Materials, and Software Availability. Raw video files and supporting data have been deposited in WashU Research Data repository (https://doi.org/10.7936/6RXS-103621) (57).

ACKNOWLEDGMENTS. This work was supported under NSF Grants No. CMMI-1633971 and CBET-1944063. The authors acknowledge use of the Institute of Materials Science and Engineering microfabrication facility at Washington University in St. Louis. Special thanks go to Jianxing Sun and the Weisensee Lab for discussion of and access to the high-speed imaging setup. Gervette Penny and the Dutcher Lab and Ye Bi and the Fields Lab provided *C. reinhardtii* cells and tumor cell lines, respectively.

Author affiliations: [a]Department of Mechanical Engineering and Materials Science, Washington University in St. Louis, St. Louis, MO 63130; [b]Research Laboratory of Electronics, Massachusetts Institute of Technology, Cambridge, MA 02139; and [c]Department of Genetics, Washington University School of Medicine in St. Louis, St. Louis, MO 63110

1. G. J. Pazour *et al.*, Identification of predicted human outer dynein arm genes: Candidates for primary ciliary dyskinesia genes. *J. Med. Genet.* **43**, 62–73 (2006).
2. M. Gui *et al.*, Structures of radial spokes and associated complexes important for ciliary motility. *Nat. Struct. Mol. Biol.* **28**, 29–37 (2021).
3. A. Horani *et al.*, Establishment of the early cilia preassembly protein complex during motile ciliogenesis. *Proc. Natl. Acad. Sci. U.S.A.* **115**, E1221–E1228 (2018).
4. S. T. Christensen *et al.*, Sensory cilia and integration of signal transduction in human health and disease. *Traffic* **8**, 97–109 (2007).
5. J. F. Reiter, M. R. Leroux, Genes and molecular pathways underpinning ciliopathies. *Nat. Rev. Mol. Cell Biol.* **18**, 533–547 (2017).
6. M. W. Leigh *et al.*, Clinical and genetic aspects of primary ciliary dyskinesia/Kartagener syndrome. *Genet. Med.* **11**, 473–487 (2009).
7. D. Nicastro *et al.*, The molecular architecture of axonemes revealed by cryoelectron tomography. *Science* **313**, 944–948 (2006).
8. I. Ibañez-Tallon *et al.*, Dysfunction of axonemal dynein heavy chain Mdnah5 inhibits ependymal flow and reveals a novel mechanism for hydrocephalus formation. *Hum. Mol. Genet.* **13**, 2133–2141 (2004).
9. S. S. Merchant *et al.*, The Chlamydomonas genome reveals the evolution of key animal and plant functions. *Science* **318**, 245–250 (2007).
10. V. F. Geyer *et al.*, Cell-body rocking is a dominant mechanism for flagellar synchronization in a swimming alga. *Proc. Natl. Acad. Sci. U.S.A.* **110**, 18058–18063 (2013).
11. V. F. Geyer *et al.*, Independent control of the static and dynamic components of the Chlamydomonas flagellar beat. *Curr. Biol.* **26**, 1098–1103 (2016).
12. U. Rüffer, W. Nultsch, High-speed cinematographic analysis of the movement of Chlamydomonas. *Cell Motil.* **5**, 251–263 (1985).
13. K. Schaller, R. David, R. Uhl, How Chlamydomonas keeps track of the light once it has reached the right phototactic orientation. *Biophys. J.* **73**, 1562–1572 (1997).
14. D. Cortese, K. Y. Wan, Control of helical navigation by three-dimensional flagellar beating. *Phys. Rev. Lett.* **126**, 088003 (2021).
15. D. R. Brumley *et al.*, Flagellar synchronization through direct hydrodynamic interactions. *Elife* **3**, e02750 (2014).
16. K. Y. Wan, R. E. Goldstein, Coordinated beating of algal flagella is mediated by basal coupling. *Proc. Natl. Acad. Sci. U.S.A.* **113**, E2784–E2793 (2016).
17. A. Ashkin *et al.*, Observation of a single-beam gradient force optical trap for dielectric particles. *Opt. Lett.* **11**, 288–290 (1986).
18. T. L. Min *et al.*, High-resolution, long-term characterization of bacterial motility using optical tweezers. *Nat. Methods* **6**, 831–835 (2009).
19. Z. Zhang, T. E. Kimkes, M. Heinemann, Manipulating rod-shaped bacteria with optical tweezers. *Sci. Rep.* **9**, 1–9 (2019).
20. C. Jones *et al.*, Stochastic force dynamics of the model microswimmer Chlamydomonas reinhardtii: Active forces and energetics. *Phys. Rev. E.* **103**, 032403 (2021).
21. E. J. Peterman, F. Gittes, C. F. Schmidt, Laser-induced heating in optical traps. *Biophys. J.* **84**, 1308–1316 (2003).
22. P. Daldrop *et al.*, Extending the range for force calibration in magnetic tweezers. *Biophys. J.* **108**, 2550–2561 (2015).
23. M. M. Van Oene *et al.*, Biological magnetometry: Torque on superparamagnetic beads in magnetic fields. *Phys. Rev. Lett.* **114**, 218301 (2015).
24. M. Krishnan *et al.*, Geometry-induced electrostatic trapping of nanometric objects in a fluid. *Nature* **467**, 692–695 (2010).
25. P. Zhang *et al.*, Acoustoelectronic nanotweezers enable dynamic and large-scale control of nanomaterials. *Nat. Commun.* **12**, 1–10 (2021).
26. N. G. Durmus *et al.*, Magnetic levitation of single cells. *Proc. Natl. Acad. Sci. U.S.A.* **112**, E3661–E3668 (2015).
27. H. Itoh *et al.*, Mechanically driven ATP synthesis by F 1-ATPase. *Nature* **427**, 465–468 (2004).
28. Q. Li *et al.*, Programmed magnetic manipulation of vesicles into spatially coded prototissue architectures arrays. *Nat. Commun.* **11**, 1–9 (2020).
29. Y. Wan *et al.*, Rapid magnetic isolation of extracellular vesicles via lipid-based nanoprobes. *Nat. Biomed. Eng.* **1**, 1–11 (2017).
30. E. Ruiz-Hernandez, A. Baeza, M. Vallet-Regi, Smart drug delivery through DNA/magnetic nanoparticle gates. *ACS Nano* **5**, 1259–1266 (2011).
31. A. Snezhko, I. S. Aranson, Magnetic manipulation of self-assembled colloidal asters. *Nat. Mater* **10**, 698–703 (2011).
32. A. Mishra *et al.*, Ultrahigh-throughput magnetic sorting of large blood volumes for epitope-agnostic isolation of circulating tumor cells. *Proc. Natl. Acad. Sci. U.S.A.* **117**, 16839–16847 (2020).
33. F. Guo *et al.*, Three-dimensional manipulation of single cells using surface acoustic waves. *Proc. Natl. Acad. Sci. U.S.A.* **113**, 1522–1527 (2016).
34. J. Shi *et al.*, Acoustic tweezers: Patterning cells and microparticles using standing surface acoustic waves (SSAW). *Lab Chip* **9**, 2890–2895 (2009).
35. M. Wu *et al.*, Isolation of exosomes from whole blood by integrating acoustics and microfluidics. *Proc. Natl. Acad. Sci. U.S.A.* **114**, 10584–10589 (2017).
36. S. Yang *et al.*, Harmonic acoustics for dynamic and selective particle manipulation. *Nat. Mater.* **21**, 540–546 (2022).
37. D. J. Collins *et al.*, Two-dimensional single-cell patterning with one cell per well driven by surface acoustic waves. *Nat. Commun.* **6**, 8686 (2015).
38. W. Connacher *et al.*, Micro/nano acoustofluidics: Materials, phenomena, design, devices, and applications. *Lab Chip* **18**, 1952–1996 (2018).
39. J. Friend, L. Y. Yeo, Microscale acoustofluidics: Microfluidics driven via acoustics and ultrasonics. *Rev. Mod. Phys.* **83**, 647 (2011).
40. X. Ding *et al.*, On-chip manipulation of single microparticles, cells, and organisms using surface acoustic waves. *Proc. Natl. Acad. Sci. U.S.A.* **109**, 11105–11109 (2012).
41. S. C. Takatori *et al.*, Acoustic trapping of active matter. *Nat. Commun.* **7**, 10694 (2016).
42. M. Kim *et al.*, Acoustic trap-and-release for rapid assessment of cell motility. *Soft Matter* **15**, 4266–4275 (2019).
43. M. Kim, P. V. Bayly, J. M. Meacham, Motile cells as probes for characterizing acoustofluidic devices. *Lab Chip* **21**, 521–533 (2021).
44. M. Cui *et al.*, Thermal considerations for microswimmer trap-and-release using standing surface acoustic waves. *Lab Chip* **21**, 2534–2543 (2021).
45. M. Bottier *et al.*, How does cilium length affect beating? *Biophys. J.* **116**, 1292–1304 (2019).
46. M. Kim, R. Barnkob, J. M. Meacham, Rapid measurement of the local pressure amplitude in microchannel acoustophoresis using motile cells. *J. Acoust. Soc. Am.* **150**, 1565–1576 (2021).
47. M. Barmatz, P. Collas, Acoustic radiation potential on a sphere in plane, cylindrical, and spherical standing wave fields. *J. Acoust. Soc. Am.* **77**, 928–945 (1985).
48. M. Schroda, D. Hemme, T. Mühlhaus, The Chlamydomonas heat stress response. *Plant J.* **82**, 466–480 (2015).
49. K. Y. Wan, K. C. Leptos, R. E. Goldstein, Lag, lock, sync, slip: The many 'phases' of coupled flagella. *J. R. Soc. Interface* **11**, 20131160 (2014).
50. K. C. Leptos *et al.*, Antiphase synchronization in a flagellar-dominance mutant of Chlamydomonas. *Phys. Rev. Lett.* **111**, 158101 (2013).
51. B. Huang *et al.*, Uniflagellar mutants of Chlamydomonas: Evidence for the role of basal bodies in transmission of positional information. *Cell* **29**, 745–753 (1982).
52. K. Foster, R. Smyth, Light antennas in phototactic algae. *Microbiol. Rev.* **44**, 572–630 (1980).
53. R. Rikmenspoel, Movements and active moments of bull sperm flagella as a function of temperature and viscosity. *J. Exp. Biol.* **108**, 205–230 (1984).
54. T. Yagi *et al.*, An axonemal dynein particularly important for flagellar movement at high viscosity: Implications from a new Chlamydomonas mutant deficient in the dynein heavy chain gene DHC9. *J. Biol. Chem.* **280**, 41412–41420 (2005).
55. K. S. Wilson *et al.*, Dynein-deficient flagella respond to increased viscosity with contrasting changes in power and recovery strokes. *Cytoskeleton* **72**, 477–490 (2015).
56. V. F. Geyer, J. Howard, P. Sartori, Ciliary beating patterns map onto a low-dimensional behavioural space. *Nat. Phys.* **18**, 332–337 (2022).
57. M. Cui *et al.*, Robust acoustic trapping and perturbation of single-cell microswimmers illuminate three-dimensional swimming and ciliary coordination [dataset]. WashU Research Data. https://doi.org/10.7936/6RXS-103621. Deposited 5 May 2023.